

Electromagnetic Scattering From a Rough Layer: Propagation-Inside-Layer Expansion Method Combined to the Forward-Backward Novel Spectral Acceleration

Nicolas Déchamps and Christophe Bourlier, *Member, IEEE*

Abstract—In this paper, an efficient method is developed to calculate the bistatic cross section (BSC) from a stack of two one-dimensional rough interfaces separating homogeneous media. The PILE (propagation-inside-layer expansion) method recently developed by Déchamps *et al.* was efficient with a complexity $\mathcal{O}(N^2)$ (N being the number of samples per interface). To reduce this complexity, a fast method valid for a single rough surface, the forward-backward with novel spectral acceleration (FBNSA) is combined to the PILE method. Furthermore, the calculation of the coupling interactions between both interfaces are also accelerated using the NSA. The PILE-FBNSA method reaches then a complexity of only $\mathcal{O}(N)$. A study of the convergence of the PILE is done and compared to the FBNSA of Moss *et al.*

Index Terms—Electromagnetic scattering from rough surfaces, forward-backward, layered surfaces, method of moments (MoM), novel spectral acceleration (NSA), propagation-inside-layer expansion (PILE) method.

I. INTRODUCTION

THE study of electromagnetic scattering from a stack of two one-dimensional rough interfaces separating homogeneous media has a large number of applications: for example, in optics for coated surfaces, [1]–[7], in near-field microscopy [8], in remote sensing for the monitoring of oil spills [9]–[11] and in the detection of buried interfaces (e.g., in sediments) using ground-penetrating radar [12].

Both approximate and rigorous methods have been developed for 20 years to tackle this problem, but they are far less numerous than for the single-interface problem. Among the approximate methods some are based on a small perturbation method [13], on the reduced Rayleigh equations [14], both of them limited to small root-mean-square deviation of heights (rms heights) of the interfaces, comparatively to the wavelength. Recently, the geometrical optics approximation has been extended to a rough layer [17] and requires quite large rms heights. We can also quote the recent method [15], [16], which

assumes “localized roughness” and devoted to cylindrical bodies buried beneath a rough interface.

The rigorous numerical approach is more recent, due to the great number of unknowns in the double-interface configuration. Thus, only a few methods have been devoted to obtain a rigorous solution: one based on the propagation-inside-layer expansion (PILE) approach [18], one based on the extended boundary condition method (EBCM) [19], another one based on the forward-backward novel spectral acceleration (FBNSA) [20] and a last one using the steepest descent fast multipole method (SDFMM) [21]. Nevertheless, these methods have still some constraints: the method in [19] is limited to small rms heights; in the case of [21] “the depth of the underground interface should be less than one free-space wavelength to satisfy the quasiplanar structure constraint of the SDFMM.” In the case of [20], the convergence domain of the method is still unclear, in particular, concerning configurations where guided waves exist. Finally, the method in [18] is slow comparatively to the other ones (complexity of $\mathcal{O}(N^2)$ versus $\mathcal{O}(N \log N)$ and less, where N is the number of samples per interface).

To overcome this limitation, we propose a fast numerical method improving PILE approach [18], which is devoted to efficiently compute the scattering from a stack of two one-dimensional (1-D) rough interfaces, and with a complexity $\mathcal{O}(N)$. This method is not restricted to small rms heights nor small thicknesses H . The main advantage of PILE, obtained from the integral equations and the method of moments (MoM) [22], [23], is that it breaks up the resolution of the linear system into different steps; two dedicated to solve for the local interactions on the surfaces and two other ones focused on the coupling. Thus it allows the use of efficient methods valid for a single rough interface [24], [25] to calculate the local interactions. In this paper, PILE is improved by adapting one fast method, the novel spectral acceleration (NSA) to both the local interactions and the coupling steps.

This paper is organized as follows: in Section II the PILE algorithm is briefly reminded. Section III focus on the NSA for a single interface, that is used to solve for the local interactions on each interface; the notations introduced there are helpful to clarify in Section IV, where the coupling step of PILE is accelerated with a new method. In Section V, the convergence of the accelerated PILE method is investigated, and next, comparisons with a rigorous [20] method of the literature is presented.

Manuscript received February 20, 2007; revised July 30, 2007.

N. Déchamps and C. Bourlier are with the Radar Team, Institut de Recherche en Electrotechnique et Electronique de Nantes Atlantique of Polytech’Nantes, 44306 Nantes, France (e-mail: christophe.bourlier@univ-nantes.fr).

Digital Object Identifier 10.1109/TAP.2007.910360

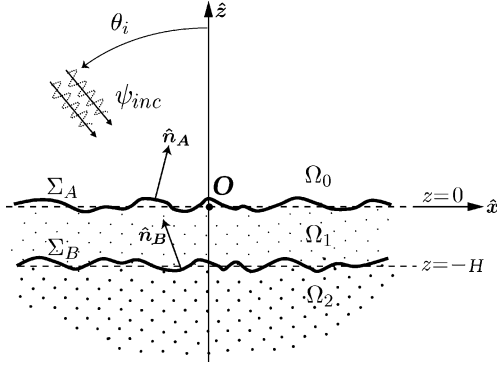


Fig. 1. Scattering from two rough interfaces Σ_A and Σ_B separating homogeneous media.

II. PILE METHOD

A. Geometry of the Problem

Let us assume that the rough layer is invariant along the \hat{y} direction and that the incident wave vector is lying in the (\hat{x}, \hat{z}) plane. Consequently, the problem is two-dimensional and the layer is delimited by two one-dimensional surfaces: an upper one, Σ_A defined by the surface equation $z = \zeta^A(x)$, and a lower one, Σ_B , defined by ζ^B (Fig. 1). $\zeta^{A,B}$ are assumed to be stochastic, stationary, Gaussian processes, satisfying $\langle \zeta^A \rangle = 0$ and $\langle \zeta^B \rangle = -H$, where $H > 0$ is the mean thickness of the layer; the surface height spectrum can be of any kind: Gaussian, West-O'Donnell [26]. If the surfaces are not identical, one must pay a special attention to avoid any intersection between them.

The random surfaces $\Sigma_{A,B}$ can easily be generated by a spectral method, widely used in the calculation of wave scattering [23]. If N represents the number of samples for each surface, discretized abscissa and heights of the surfaces are given by

$$x_n = -\frac{L}{2} + \left(n - \frac{1}{2}\right) \Delta x \quad \text{and} \quad \zeta^{A,B}(x_n) \quad n=1 \dots N \quad (1)$$

where $\Delta x = L/N$ is the sampling step and L is the total length of each surface. A point of the plane (\hat{x}, \hat{z}) will be denoted by $\mathbf{r} = x\hat{x} + z\hat{z}$ and a point belonging to $\Sigma_{A,B}$ by $\mathbf{r}_n^{A,B} = x_n\hat{x} + \zeta^{A,B}(x_n)\hat{z}$. For sake of clarity, will let $\zeta_n^{A,B} = \zeta^{A,B}(x_n)$.

The surfaces separate three homogeneous media: the upper one, Ω_0 , considered as air, the intermediate one, filling the layer, Ω_1 , and the lower one, Ω_2 . Ω_2 will be considered as a lossy dielectric or a perfect conductor, and we will denote the corresponding configuration, for sake of simplicity, dielectric case or perfectly conducting case, respectively. The wave number in the medium Ω_i will be denoted k_i .

To avoid edge limitations, the incident field ψ_{inc} is chosen as a Thorsos' tapered plane wave [27]. Let us denote θ_i the incident angle, defined with respect to \hat{z} in the counterclockwise direction, and g the tapering parameter, which has a dimension of length and controls the spatial extent of the incident wave. Typically, g is chosen to be some fraction of L ; we used $g = L/6$ or $g = L/10$ in numerical simulations. Furthermore, we consider

both TE (or s) and TM (or p) polarizations. An $e^{j\omega t}$ time-harmonic convention is used.

B. PILE Method

This new method has been recently developed by Déchamps *et al.* in [18] and was thoroughly studied in this paper. The main equations are given.

An integral method combined to the MoM leads to a linear system expressed as [22], [18]

$$\mathbf{Z}\mathbf{X} = \mathbf{s} \quad (2)$$

where \mathbf{Z} is the impedance matrix. The unknown vector \mathbf{X} is equal to

$$\mathbf{X} = \begin{bmatrix} \mathbf{X}_A \\ \mathbf{X}_B \end{bmatrix} \quad (3)$$

with \mathbf{X}_A and \mathbf{X}_B containing the unknown fields $\psi_{A,B}$ and their normal derivatives $\partial\psi_{A,B}/\partial n_{A,B}$ on the upper and lower surfaces, respectively. For example

$$\mathbf{X}_A^t = \left[\psi_A(\mathbf{r}_1^A) \dots \psi_A(\mathbf{r}_N^A) \frac{\partial\psi_A(\mathbf{r}_1^A)}{\partial n_A} \dots \frac{\partial\psi_A(\mathbf{r}_N^A)}{\partial n_A} \right] \quad (4)$$

where \cdot^t denotes the transpose operator. \mathbf{X}_B has a similar arrangement of terms. The source term \mathbf{s} contains information about the incident field

$$\mathbf{s} = \begin{bmatrix} \mathbf{s}_A \\ \mathbf{s}_B \end{bmatrix} = \begin{bmatrix} \mathbf{s}_A \\ \mathbf{0} \end{bmatrix} \quad (5)$$

with

$$\mathbf{s}_A^t = [\psi_{\text{inc}}(\mathbf{r}_1^A) \dots \psi_{\text{inc}}(\mathbf{r}_N^A) 0 \dots 0] \quad (6)$$

and $\mathbf{s}_B = \mathbf{0}$, because the incident field only illuminates the upper surface.

To solve efficiently the linear system, we take advantage of the block partitioning of the impedance matrix \mathbf{Z} which has the form [18]

$$\mathbf{Z} = \begin{bmatrix} \mathbf{Z}^A & \mathbf{C}^{B \rightarrow A} \\ \mathbf{C}^{A \rightarrow B} & \mathbf{Z}^B \end{bmatrix} \quad (7)$$

\mathbf{Z}^A exactly corresponds to the impedance matrix of a single-interface problem, where the surface considered is the upper one, Σ_A . Likewise, \mathbf{Z}^B is the impedance matrix of the single lower surface, Σ_B . Matrices $\mathbf{C}^{B \rightarrow A}$ and $\mathbf{C}^{A \rightarrow B}$ can be seen as coupling matrices between the two interfaces Σ_A and Σ_B . The complete expression of these matrices can be found in [43, Appendix 1].

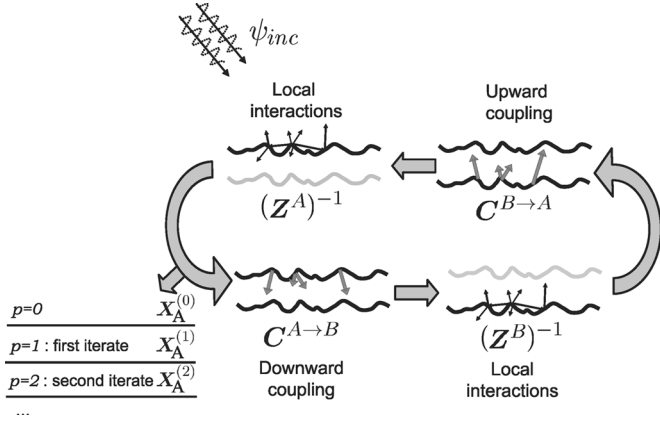


Fig. 2. Physical interpretation of the PILE method; each factor of the product $\mathbf{Y}_A^{(p)} = (\mathbf{Z}^A)^{-1} \cdot \mathbf{C}^{B \rightarrow A} \cdot (\mathbf{Z}^B)^{-1} \cdot \mathbf{C}^{A \rightarrow B} \cdot \mathbf{Y}_A^{(p-1)}$ has a particular function in the scheme. In the zeroth order term, $(\mathbf{Z}^A)^{-1}$ accounts for the local interactions on the upper interface, so $\mathbf{Y}_A^{(0)}$ corresponds to the contribution of the direct reflection on the upper surface, without entering inside the layer. In the first order term, $\mathbf{Y}_A^{(1)} = \mathbf{M}_c \cdot \mathbf{Y}_A^{(0)}$, $\mathbf{C}^{A \rightarrow B}$ propagates the resulting upper field information, $\mathbf{Y}_A^{(0)}$, toward the lower interface, $(\mathbf{Z}^B)^{-1}$ accounts for the local interactions on the lower interface, and $\mathbf{C}^{B \rightarrow A}$ repropagates the resulting contribution toward the upper interface; finally, $(\mathbf{Z}^A)^{-1}$ updates the field values on the upper interface.

As we usually compute the scattering field in the upper medium, only the upper scattered field \mathbf{X}_A is needed. It is approximated by [18]

$$\mathbf{X}_A^{(P_{\text{pile}})} = \left[\sum_{p=0}^{P_{\text{pile}}} \mathbf{M}_c^p \right] \cdot (\mathbf{Z}^A)^{-1} \cdot \mathbf{s}_A = \sum_{p=0}^P \mathbf{Y}_A^{(p)} \quad (8)$$

in which

$$\begin{aligned} \mathbf{Y}_A^{(0)} &= (\mathbf{Z}^A)^{-1} \cdot \mathbf{s}_A \text{ for } p = 0 \\ \mathbf{Y}_A^{(p)} &= \mathbf{M}_c \cdot \mathbf{Y}_A^{(p-1)} \text{ for } p > 0 \end{aligned} \quad (9)$$

and \mathbf{M}_c is the characteristic matrix of the layer defined as

$$\mathbf{M}_c = (\mathbf{Z}^A)^{-1} \cdot \mathbf{C}^{B \rightarrow A} \cdot (\mathbf{Z}^B)^{-1} \cdot \mathbf{C}^{A \rightarrow B}. \quad (10)$$

We define the norm $\|\mathbf{M}_c\|$ of a complex matrix by its spectral radius, i.e., the modulus of its eigenvalue which has the highest modulus. Expansion (8) is accurate if $\|\mathbf{M}_c\|$ is inferior to 1. The physical interpretation of \mathbf{M}_c is shown in Fig. 2.

The advantage of the PILE method [cf. (8)], is that the most complex operations, which are $(\mathbf{Z}^A)^{-1} \cdot \mathbf{u}$ and $(\mathbf{Z}^B)^{-1} \cdot \mathbf{u}$ (where \mathbf{u} is a vector), only concerns the local interactions on each surface, respectively upper and lower, and can be calculated by fast numerical methods that already exist for a single rough surface, like for instance the banded matrix iterative approach/canonical grid (BMIA/CAG) [32]–[36], the fast multipole method (FMM) [37] or the forward-backward/NSA method (FBNSA) [38]–[41]. Let us recall that the advantage

TABLE I
EXAMPLES OF METHODS THAT CAN BE USED TO SPEED UP THE OPERATION $(\mathbf{Z})^{-1} \cdot \mathbf{v}$. COMPLEXITY WITH \mathbf{Z} OF DIMENSION $N \times N$

Method	Complexity
LU inversion	$\mathcal{O}(N^3)$
FB	$\mathcal{O}(N^2)$
One Level FMM	$\mathcal{O}(N^{3/2})$
Multilevel FMM	$\mathcal{O}(N \log N)$
BMIA/CAG	$\mathcal{O}(N \log N)$
SDFMM	$\mathcal{O}(N)$
FBNSA	$\mathcal{O}(N)$

of all the above methods is that $(\mathbf{Z})^{-1}$ is never explicitly calculated.

III. COMPUTATION OF THE LOCAL INTERACTIONS WITH THE FBNSA

Hence, applying one of the fast methods quoted before can speed up the calculations $(\mathbf{Z}^A)^{-1} \cdot \mathbf{u}$ and $(\mathbf{Z}^B)^{-1} \cdot \mathbf{u}$ and can reduce the complexity of both steps to less than $\mathcal{O}(N^2)$. Table I summarizes the complexity of each available method.

Let us apply the NSA combined originally to the forward-backward to reduce the complexity of these products. The NSA is one of the most promising acceleration techniques to solve diffraction from rough surfaces. What makes it attractive is its complexity of only $\mathcal{O}(N)$ and its relatively simple algorithm, easy to program. A detailed presentation can be found in [39], [41].

The FBNSA was originally developed for a single perfectly conducting interface (PC), in both TE and TM polarizations [39], [41]. A quick reminder of the method will be given hereafter for these configurations. The FBNSA for a lower media very conducting (impedance boundary condition) was also derived [39]. The notations introduced here will be useful for the reader to deduce the FBNSA formulas for the dielectric single-interface case and most of all, to develop the formulas for the coupling step. Fig. 3 gathers all the configurations studied. The NSA method for the dielectric single-interface case (b) can be derived from the PC single-interface case (a), because of the particular structure of the impedance matrix for the dielectric case. In the same way, the NSA for the coupling step (c) and (d) can be derived from case (a).

The FB algorithm is based on the following decomposition

$$\begin{cases} \mathbf{Z} = \mathbf{Z}^f + \mathbf{Z}^d + \mathbf{Z}^b \\ \mathbf{X} = \mathbf{X}^b + \mathbf{X}^f \end{cases} \quad (11)$$

where \mathbf{Z}^f , \mathbf{Z}^b and \mathbf{Z}^d are lower triangular, upper triangular and diagonal matrices, respectively. \mathbf{X}^b and \mathbf{X}^f are two vectors linked to the contributions forward (from the points on the left of the current point) and backward (from the right), respectively. The surface is oriented by assuming that the incident beam propagates from the left to the right. Fig. 4 shows a physical interpretation of the matrices \mathbf{Z}^f and \mathbf{Z}^b . \mathbf{X}^b and \mathbf{X}^f are the con-

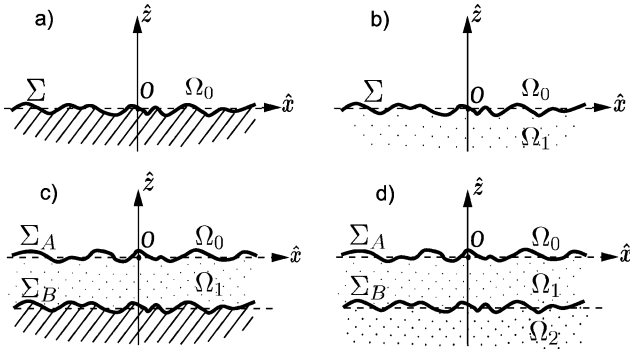


Fig. 3. Illustration of the different notations used in the paper: (a) perfectly-conducting (PC) single interface, (b) dielectric single interface, (c) PC layer, (d) dielectric layer.

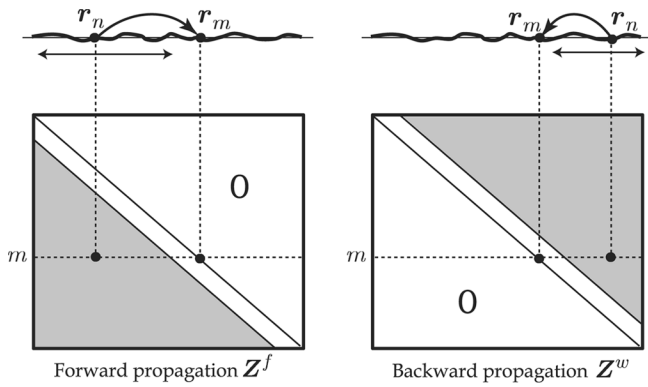


Fig. 4. Physical interpretation of the multiplication by forward and backward matrices \mathbf{Z}^f and \mathbf{Z}^b , respectively. \mathbf{r}_m is the observation (current) point and \mathbf{r}_n the source point; $Z_{mn}^{b,f}$ propagates the field from \mathbf{r}_n to \mathbf{r}_m .

vergent solution of the following system, supposed equivalent to $\mathbf{Z}\mathbf{X} = \mathbf{s}$:

$$\begin{cases} \mathbf{Z}^d \mathbf{X}^f = \mathbf{s} - \mathbf{Z}^f (\mathbf{X}^b + \mathbf{X}^f) \\ \mathbf{Z}^d \mathbf{X}^b = -\mathbf{Z}^b (\mathbf{X}^b + \mathbf{X}^f) \end{cases} \quad (12)$$

where \mathbf{s} is the source term for a single PC interface

$$\mathbf{s}^t = [\psi_{inc}(\mathbf{r}_1) \dots \psi_{inc}(\mathbf{r}_N)]. \quad (13)$$

In (12), the resolution is done iteratively: assuming first $\mathbf{X}^b = \mathbf{0}$, the first equation of (12) is solved for \mathbf{X}^f ; then introducing \mathbf{X}^f in the second equation of (12), \mathbf{X}^b is found. The first iterate $\mathbf{X}^{(0)}$ is then calculated by $\mathbf{X}^{(0)} = \mathbf{X}^f + \mathbf{X}^b$. The scheme is repeated again to find the next iterates $\mathbf{X}^{(1 \dots p)}$.

Actually, the way (12) is cast is very convenient to solve by substitution for \mathbf{X}^f and \mathbf{X}^b ; because \mathbf{Z}^f is lower triangular with null diagonal coefficients, we get $X_1^f = s_1/Z_{11}^d$; $X_2^f = [s_2 - Z_{21}^f (X_1^f + X_1^b)]/Z_{22}^d$, and so on. The m th coefficient is given by

$$X_m^f = \left[s_m - \sum_{n=1}^{m-1} Z_{mn}^f (X_n^f + X_n^b) \right] / Z_{mm}^d. \quad (14)$$

Similarly $X_N^b = 0$; $X_{N-1}^b = -Z_{N-1,N}^f (X_N^f + X_N^b)/Z_{N,N}^d$, and so on. For the m th coefficient

$$X_m^b = \left[- \sum_{n=m+1}^N Z_{mn}^b (X_n^f + X_n^b) \right] / Z_{mm}^d. \quad (15)$$

The NSA is used to speed up the resolution of both equations of (12) for \mathbf{X}^f and \mathbf{X}^b , respectively. More precisely, the NSA can speed up the product $\mathbf{Z}^f \mathbf{v}$ and $\mathbf{Z}^b \mathbf{v}$ where \mathbf{v} is any vector. For example, when performing the product $\mathbf{Z}\mathbf{v} = \mathbf{u}$ with \mathbf{Z} lower or upper triangular, the number of multiplications to find the elements $(\mathbf{u})_{m=1,2,\dots,N}$ in a row is $1 + 2 + 3 + \dots + N = \mathcal{O}(N^2)$. With the NSA, only $\mathcal{O}(N)$ multiplications are needed. In the next section the basic concept of the NSA is recalled. A more detailed theory can be found in [39], [41].

A. TE Single-Interface Perfectly Conducting Case

Let us consider two points $(\mathbf{r}_m, \mathbf{r}_n)$ belonging to the same surface Σ and let us denote $x_d = x_m - x_n$ and $z_d = \zeta_m - \zeta_n$. \mathbf{r}_m is the observation point, fixed, and \mathbf{r}_n the source point, that moves on the surface. The total impedance matrix \mathbf{Z} as in (11) in this configuration has the same expression than $\mathbf{B}^{A,B}$ in [43, Appendix I]. In the TE case, let $v_n = X_n^f + X_n^b$, and let include the $\gamma_n = \sqrt{1 + (\zeta_n')^2}$ coefficient of $\mathbf{B}^{A,B}$ as a factor in the unknown v_n . Accordingly, the off-diagonal elements are

$$Z_{mn} = \Delta x g(\mathbf{r}_m, \mathbf{r}_n) \text{ for } n \neq m. \quad (16)$$

where $g(\mathbf{r}_m, \mathbf{r}_n) = (i/4)H_0^{(1)}(k\|\mathbf{r}_m - \mathbf{r}_n\|)$ is the 2-D Green function in free space and $H_0^{(1)}$ is the Hankel function from the first kind of order zero. Let x_{d0} be the horizontal distance separating the weak interactions from the strong, and let N_s be the integer part $[\cdot]$ of $x_{d0}/\Delta x$. Then, considering first the forward case, the sum from (14) can be cast into, for $m > N_s + 1$

$$\begin{aligned} \sum_{n=1}^{m-1} Z_{mn}^f v_n &= \sum_{n=1}^{m-N_s-1} Z_{mn}^{f,(w)} v_n + \sum_{n=m-N_s}^{m-1} Z_{mn}^{f,(s)} v_n \\ &= E_m^{f,(w)} + E_m^{f,(s)}. \end{aligned} \quad (17)$$

In the above decomposition the term $E_m^{f,(s)}$ is performed exactly for each $m > N_s + 1$, whereas $E_m^{f,(w)}$ is calculated using the NSA. The NSA is based on the following decomposition of the Green function, written here for $x_m - x_n > 0$ [39], [41]

$$g(\mathbf{r}_m, \mathbf{r}_n) = \frac{i}{4\pi} \int_C e^{ik[(x_m - x_n) \cos \phi + (\zeta_m - \zeta_n) \sin \phi]} d\phi \quad (18)$$

where $C = [-(\pi/2 + j\infty); -(\pi/2)[\cup[-(\pi/2); +(\pi/2)]] \cup [(\pi/2); +(\pi/2) - j\infty]$. This path is usually replaced by a steepest descent path $C_{\{m,n\}}$, going through the saddle point $\phi_{smn}^s = \arctan[(\zeta_n - \zeta_m/x_n - x_m)] \in [-\pi/2; +\pi/2]$. The group of paths $\{C_{\{m,n\}}\}$ associated to all couple of points $(\mathbf{r}_m, \mathbf{r}_n)$ can be replaced by an unique path C_δ going through the origin; furthermore, close to the origin, C_δ is a straight line having a slope $-\tan \delta$. If δ is correctly chosen, the integrand of (18) decays rapidly away from the origin and the phase has little

variations. Thus, as in a classical saddle-point technique, after changing C by C_δ in (18), the integration over ϕ can be approximated by a sum over a limited number of complex angles $\{\phi_p, p = -Q..Q\}$. That is, introducing (16) and (18) into (17) we get

$$\begin{aligned} E_m^{f,(w)} &= \sum_{n=1}^{m-N_s-1} \Delta x g(\mathbf{r}_m, \mathbf{r}_n) v_n \\ &= \frac{i\Delta x}{4\pi} \sum_{n=1}^{m-N_s-1} v_n \\ &\quad \times \int_{C_\delta} e^{ik[(x_m-x_n)\cos\phi + (\zeta_m-\zeta_n)\sin\phi]} d\phi \\ &= \frac{i\Delta x}{4\pi} \int_{C_\delta} F_m(\phi) e^{ik\zeta_m \sin\phi} d\phi \\ &= \frac{i\Delta x}{4\pi} e^{-i\delta} \sum_{p=-Q}^{+Q} F_m(\phi_p) e^{ik\zeta_m \sin\phi_p} \Delta\phi \end{aligned} \quad (19)$$

with

$$F_m(\phi) = \sum_{n=1}^{m-N_s-1} v_n e^{ik[(x_m-x_n)\cos\phi - \zeta_n \sin\phi]}. \quad (20)$$

The advantage is that $F_m(\phi)$ can be calculated from $F_{m-1}(\phi)$ by

$$F_m(\phi) = F_{m-1}(\phi) e^{ik\Delta x \cos\phi} + v_{m-N_s-1} e^{ik[(N_s+1)\Delta x \cos\phi - \zeta_{m-N_s-1} \sin\phi]}. \quad (21)$$

The parameters are given by [39]

$$\begin{aligned} R_s &= \sqrt{x_{d0}^2 + (\zeta_{max} - \zeta_{min})^2} \\ \Delta\phi &= \frac{1}{22} \sqrt{\frac{5}{kR_s}} \\ \phi_{s,max} &= \arctan \left[\frac{\zeta_{max} - \zeta_{min}}{x_{d0}} \right] \\ \beta_s &= \sqrt{\frac{10}{kx_{d0}}} \\ \delta &= \arctan \left[\min \left(\frac{20}{kR_s \phi_{s,max}^2}; 1 \right) \right] \\ Q &= \left\lfloor \frac{\beta_s}{\Delta\phi} + 5 \right\rfloor \end{aligned} \quad (22)$$

and

$$\phi_p = p\Delta\phi e^{-i\delta} \quad (23)$$

where $\zeta_{max} = \max_{k=1..N}(\zeta_k)$ and $\zeta_{min} = \min_{k=1..N}(\zeta_k)$. The parameters rely on the choice of x_{d0} , and as a rule of thumb $x_{d0} \simeq \alpha L_c$ with $\alpha = 2$ or 3 is sufficient. A detailed study about the optimal choice for these coefficients can be found in [41].

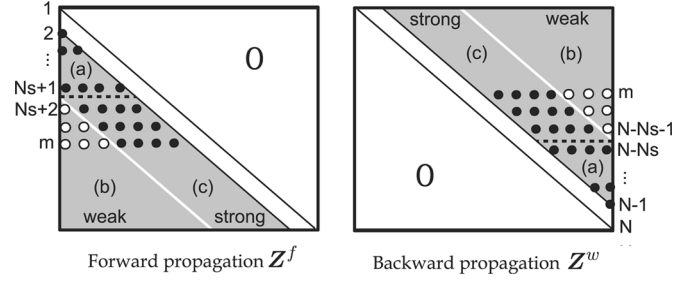


Fig. 5. Different steps during the product $\mathbf{Z}^f \mathbf{v}$ (left) and $\mathbf{Z}^b \mathbf{v}$ (right), where $\mathbf{v} = \mathbf{X}^f + \mathbf{X}^b$. First, the elements of the domain (a) are multiplied to \mathbf{v} in an exact manner. Second, the elements (b) and (c) are multiplied to \mathbf{v} , those of (b) using the NSA and those of (c) exactly like for (a).

When computing the forward step (14), the sum is performed exactly for $m = 1..N_s$ (elements (a) of Fig. 5). For each $m > N_s$ the sum is split up into two sums (17); $E_m^{f,(s)}$ is performed exactly [elements (c)] and $E_m^{f,(w)}$ is calculated using the NSA [elements (b)]. For this purpose, $F_m(\phi_p)$ is found from $F_{m-1}(\phi_p)$ for every $p = -Q..Q$ using (21), and then summed over p . Initially, $F_m(\phi_p) = 0$ for $m = 1..N_s + 1$.

The algorithm is very similar for the backward step (Fig. 5); the sum in (15) is split up into, for $m < N - N_s$

$$\begin{aligned} \sum_{n=m+1}^N Z_{mn}^b v_n &= \sum_{n=m+1}^{m+N_s} Z_{mn}^{f,(s)} v_n + \sum_{n=m+N_s+1}^N Z_{mn}^{f,(w)} v_n \\ &= E_m^{b,(s)} + E_m^{b,(w)}. \end{aligned} \quad (24)$$

$E_m^{b,(w)}$ is then rearranged as in (19). In the backward case, the main difference is that $x_m - x_n < 0$ so the decomposition of the Green function is now

$$g(\mathbf{r}_m, \mathbf{r}_n) = \frac{i}{4\pi} \int_C e^{ik[(x_m-x_n)\cos\phi - (\zeta_m-\zeta_n)\sin\phi]} d\phi. \quad (25)$$

with a negative sign in front of $(\zeta_m - \zeta_n) \sin\phi$. In a practical way, the consequence on (19), (20), and (21), is that $\cos\phi$ is unchanged but $\sin\phi \rightarrow -\sin\phi$; in (23), $\phi_p = p\Delta\phi e^{-i\delta}$ is unchanged. Furthermore, in (20) the summation goes from $m + N_s + 1$ to N , and in (21), F_m is obtained from F_{m+1} .

Because of the approximation of the integration in (18) by the previous saddle point technique and the use of the recurrent relation (21), the products $\mathbf{Z}^{f,b} \mathbf{v}$ can be computed with only $\mathcal{O}(N)$ multiplications [39].

B. TM Single-Interface Perfectly Conducting Case

The off-diagonal elements of the impedance matrix \mathbf{Z} are

$$Z_{mn} = -\Delta x \frac{\partial g(\mathbf{r}_m, \mathbf{r}_n)}{\partial n} \text{ for } n \neq m \quad (26)$$

and can be expressed with the Hankel function (see Appendix 1 of [43]; \mathbf{Z} in this case has a similar expression than $\mathbf{A}^{A,B}$). The

decomposition of the normal derivative of the Green function is, for $x_m - x_n > 0$

$$\frac{\partial g(\mathbf{r}_m, \mathbf{r}_n)}{\partial n} = \frac{-k}{4\pi} \int_C e^{ik[(x_m - x_n) \cos \phi + (\zeta_m - \zeta_n) \sin \phi]} \times [\zeta'_n \cos \phi - \sin \phi] d\phi \quad (27)$$

where ζ' is the derivate of the function defining the surface. The same algorithm than in the previous TE case can be applied for both forward and backward steps. The differences are in the expression of F_m (20) and in the recurrence relation (21)

$$F_m(\phi) = \sum_{n=1}^{m-N_s-1} [\zeta'_n \cos \phi - \sin \phi] \times v_n e^{ik[(x_m - x_n) \cos \phi - \zeta_n \sin \phi]} \quad (28)$$

and

$$F_m(\phi) = F_{m-1}(\phi) e^{ik\Delta x \cos \phi} + [\zeta'_{m-N_s-1} \cos \phi - \sin \phi] \times v_{m-N_s-1} e^{ik[(N_s+1)\Delta x \cos \phi - \zeta_{m-N_s-1} \sin \phi]} \quad (29)$$

The same term $[\zeta'_n \cos \phi - \sin \phi]$ is also applied as a factor to the backward expressions. The complexity of the NSA is also $\mathcal{O}(N)$ in the TM polarization.

C. Dielectric Case

The FB method for the single-interface dielectric case has been introduced by Iodice [42]. The decomposition (11) and the basic (12) are unchanged. The differences are on the shape of the matrices \mathbf{Z}^d , \mathbf{Z}^f and \mathbf{Z}^b , which have $2N \times 2N$ dimension, and are built up with block diagonal, block lower triangular and block upper triangular matrices, respectively. The unknowns vectors \mathbf{X}^f and \mathbf{X}^b have a dimension of $2N \times 1$. (14) and (15) are also slightly different: because in the dielectric case both the field and its normal derivative on each current point have to be found, each (14) and (15) is converted in a linear system with two equations.

To our knowledge, no article has been published for the NSA for the single-interface dielectric case, nevertheless, the task is easy once the TE and TM cases for a single PC interface have been computed, because of the particular structure of the impedance matrix for the dielectric case. The impedance matrix \mathbf{Z} in this case is similar to the \mathbf{Z}^A matrix given in Appendix 1 of [43]. In the product $\mathbf{Z}\mathbf{v}$, done by blocks, the products $\mathbf{A}^A\mathbf{v}$ and $\mathbf{C}^A\mathbf{w}$ where \mathbf{v} and \mathbf{w} are vectors, can be accelerated using the NSA for the TM PC case. In the same way, the NSA for the products $\mathbf{B}^A\mathbf{w}$ and $\mathbf{D}^A\mathbf{v}$ is directly inspired by the TE PC case. Accordingly, the FBNSA for a dielectric interface has also a complexity of $\mathcal{O}(N)$.

In Section V, the number of iterations of the FBNSA method used to speed up the local interactions in PILE, will be denoted P_{fb} .

IV. NSA FOR THE COUPLING STEP

At this point, the most penalizing steps in the calculation of (9)

$$\mathbf{Y}_A^{(p)} = (\mathbf{Z}^A)^{-1} \cdot \mathbf{C}^{B \rightarrow A} \cdot (\mathbf{Z}^B)^{-1} \cdot \mathbf{C}^{A \rightarrow B} \cdot \mathbf{Y}_A^{(p-1)}$$

are now $\mathbf{C}^{A \rightarrow B} \cdot \mathbf{v}$ and $\mathbf{C}^{B \rightarrow A} \cdot \mathbf{v}$, each one having a complexity $\mathcal{O}(N^2)$. The FB method is not useful here, because there is no matrix inversion in the coupling step. Nevertheless the NSA can be applied to speed up the product $\mathbf{C} \cdot \mathbf{u}$, where \mathbf{u} is a vector of dimension $2N \times 1$. Recently, [43], the BMIA/CAG of complexity $\mathcal{O}(N \log N)$ method and referred to as PILE + BMIA/CAG has been applied to accelerate the product $\mathbf{C} \cdot \mathbf{u}$.

For this purpose, each non-null block matrix of $\mathbf{C}^{A \rightarrow B}$ and $\mathbf{C}^{B \rightarrow A}$ are split up into a diagonal, a lower (forward) and a upper (backward) triangular matrices. For example, $\mathbf{C}^{B \rightarrow A}$ in the dielectric layer case (see Appendix 1 of [43]) is written

$$\mathbf{C}^{B \rightarrow A} = \begin{bmatrix} \mathbf{0}_{N \times N} & \mathbf{0}_{N \times N} \\ \mathbf{E} & \mathbf{F} \end{bmatrix} \quad \text{with} \quad \begin{cases} \mathbf{E} = \mathbf{E}^f + \mathbf{E}^d + \mathbf{E}^b \\ \mathbf{F} = \mathbf{F}^f + \mathbf{F}^d + \mathbf{F}^b \end{cases} \quad (30)$$

Then the product $\mathbf{C}^{B \rightarrow A} \cdot \mathbf{u}$ is performed by blocks

$$\mathbf{C}^{B \rightarrow A} \cdot \mathbf{u} = \begin{bmatrix} \mathbf{0}_{N \times 1} \\ \mathbf{E} \cdot \mathbf{u}_1 + \mathbf{F} \cdot \mathbf{u}_2 \end{bmatrix} \quad (31)$$

with $\mathbf{u} = [\mathbf{u}_1^t \mathbf{u}_2^t]^t$, and the inner products in the term on the right-hand side of (31) can be broken up into products of the kind

$$\mathbf{Z} \cdot \mathbf{v} = \mathbf{Z}^f \cdot \mathbf{v} + \mathbf{Z}^d \cdot \mathbf{v} + \mathbf{Z}^b \cdot \mathbf{v} \quad (32)$$

where $\mathbf{Z} = \mathbf{E}$ or \mathbf{F} , and $\mathbf{v} = \mathbf{u}_i$, which has a dimension $N \times 1$.

The m -element of the product (32), $(\mathbf{Z} \cdot \mathbf{v})_m$ can be written

$$(\mathbf{Z} \cdot \mathbf{v})_m = \sum_{n=1}^{m-1} Z_{mn}^f v_n + Z_{mm}^d v_m + \sum_{n=m+1}^N Z_{mn}^b v_n \quad (33)$$

and then the splittings (17) and (24) can be applied as in the PC single interface case. More precisely, the products with \mathbf{E} and \mathbf{G} are accelerated with the NSA for the TM PC case (Section III-B) and \mathbf{F} and \mathbf{H} with the NSA for the TE PC case (Section III-A). When applying the NSA, the only difference with equations of Section III-B and Section III-A, is that

$$\begin{cases} \zeta_m \rightarrow \zeta_m^A \\ \zeta_n \rightarrow \zeta_n^B \end{cases} \quad \text{for } \mathbf{E} \text{ and } \mathbf{F}, \quad \begin{cases} \zeta_m \rightarrow \zeta_m^B \\ \zeta_n \rightarrow \zeta_n^A \end{cases} \quad \text{for } \mathbf{G} \text{ and } \mathbf{H}. \quad (34)$$

To sum up, the NSA for the coupling matrices is derived as for a single interface. The parameters of the NSA are chosen as previously, with similar formulas as (22). ζ_{\max} and ζ_{\min} are substituted by $\zeta_{\max} = \max_{k=1..N}(\zeta_k^A)$ and $\zeta_{\min} = \min_{k=1..N}(\zeta_k^B)$.

The main parameter is the limit interaction length x_{d0} , or equivalently the integer $N_s^{coupl} = \lfloor x_{d0}/\Delta x \rfloor$.

V. COMPARISON WITH REFERENCES METHODS

The validity domain of the PILE method, relying on the condition $\|M_c\| < 1$, where the used norm is the spectral radius, has been studied in [18]. It is quite large, the only limitation being the poor convergence with very thin and rough layers. In Section V-A, the convergence of the PILE combined to the FBNSA (PILE-FBNSA) is investigated. To study the FB method combined to PILE method, we introduce the PILE-FB. If the NSA scheme is added, the resulting method is referred as to PILE-FBNSA.

Next, in Section V-B, we compare the PILE-FBNSA to the FBNSA developed for a layer by Moss *et al.* [20]. We call in this paper the former method FBNSA-layer to avoid any confusion. The FB-layer will denote the previous method but without the NSA acceleration. Furthermore, we point out here that the FBNSA used to speed up the PILE and the FBNSA-layer are not the same methods; the FBNSA is applied to a single interface, and the FBNSA-layer to a stack of two or more interfaces. Besides, we discuss here about three different parameters that are the orders of three different methods: P_{pile} for PILE, P_{fb} for the inner FB of PILE, and $P_{fblayer}$ for the FBNSA-layer.

Finally, in Section V-C, the computation time is studied.

In all the configurations the lower medium Ω_2 is perfectly conducting (case (c) of Fig. 3), and the relative permittivity of the inner medium Ω_1 is $\varepsilon_{r,1} = 2 + 0.01i$. Each interface, of total length $L = 50\lambda$ and with a rms slopes $\sigma_p^{A,B} = 0.2$, is sampled at $\Delta x = \lambda/10$; the surface height spectrum is Gaussian. The illuminating beam is a Thorsos beam of attenuating parameter g , and an incident angle of $\theta_i = 0^\circ$.

A. Convergence of Pile Method With FBNSA

In order to find the correct parameters to achieve a good convergence of PILE-FBNSA, we work in two steps: first, we look for the convergence of the exact PILE method, comparing it to the reference results provided by a direct inversion of the impedance matrix. More precisely we seek the minimum order P_{pile} (8) of PILE method for which the mean absolute error over $\theta_s \in [-90^\circ; 90^\circ]$ on the bistatic scattering coefficient (BSC) is less than 0.1 dB; this order, P_{pile} , corresponds to the number of prevailing reflections inside the layer. Convergence is established when a mean error of 0.1 dB or less is reached for an order P_{pile} less than 20.

Fig. 6 shows the order P_{pile} of convergence of the exact PILE, plotted versus the mean thickness H for different values of the rms heights $\sigma_h = \sigma_h^A = \sigma_h^B$, for the same rms slopes $\sigma_p^A = \sigma_p^B = 0.2$. The surfaces are supposed equal and translated from each other. The mean thickness H is chosen greater than 0.5λ , to ensure that there are enough sampling points in the layer in the vertical direction; hence the field in the layer can be appropriately modeled. The results in TM polarization are very similar. From Fig. 6, PILE method converges for all configurations, in less than four iterations for $H > 4\lambda$, and less than six iterations for $2\lambda < H < 4\lambda$.

Second, we look for an acceptable order of iteration P_{fb} of the inner FB method (used in the local interaction step of PILE).

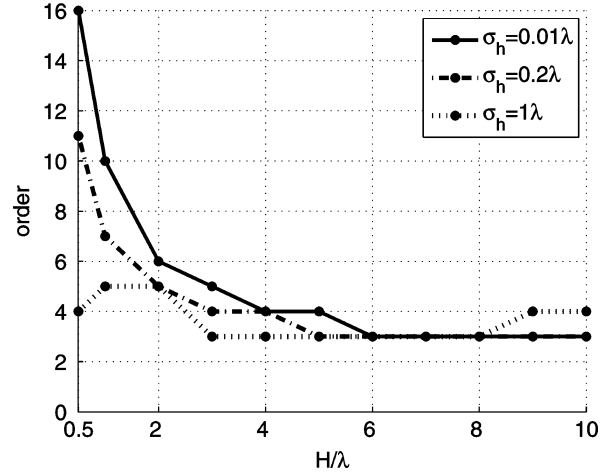


Fig. 6. Order of convergence P_{pile} of exact PILE to reach an error of 0.1 dB on the BSC. $L = 50\lambda$. Rms heights $\sigma_h = \sigma_h^A = \sigma_h^B$, rms slopes $\sigma_p^A = \sigma_p^B = 0.2$. $\theta_i = 0^\circ$. TE case. $\varepsilon_{r,1} = 2 + 0.01i$.

We follow the same procedure as before (error less than 0.1 dB on the BSC). Fig. 7 shows the error on the BSC, for two different configurations, case 1, when the convergence is slow, case 2, when the convergence is fast. The error is plotted versus both PILE order and inner FB order. For a given PILE order, the error decreases as the inner FB order increases, until it reaches a constant error value. Similarly, for a given inner FB order, the error decreases as the PILE order increases, until it reaches another constant error value. The optimal choices of P_{pile} and P_{fb} , marked by an arrow for a given error value, in Fig. 7, lie along a line (the dashed lines); with this choice, the CPU time of computation is minimum for a given error. Hence, the two parameters, P_{pile} and P_{fb} , are linked. As a rule of thumb, for all the configurations studied, PILE-FBNSA reaches an error of less than 0.1 dB on the BSC with an inner FB order of 5. Simulations not reported in this paper, showed also a good convergence of PILE-FBNSA for other values of rms slopes and rms heights.

We plotted in Fig. 8 an example of BSC obtained with an exact MoM method, the PILE-FBNSA and the FBNSA-layer method. The agreement is very good, the mean error is less than 0.1 dB.

B. Convergence of FB Method for a Layer

Because the convergence of PILE-FBNSA and FBNSA-layer is dependent on the convergence of the exact PILE and FB-layer, respectively, we focus first on a direct comparison of PILE and FB-layer methods.

Fig. 9 shows the order $P_{fblayer}$ of convergence of the FB-layer, plotted versus the mean thickness H for different values of the rms heights $\sigma_h = \sigma_h^A = \sigma_h^B$, for the same rms slopes $\sigma_p^A = \sigma_p^B = 0.2$. The surfaces are supposed equal and translated from each other. The results in TM polarization are very similar. From Fig. 9, FB-layer method converges in less than 20 iterations for $H > 2\lambda$, but does not always converge for thinner layers. Moreover, by comparison to the PILE in Fig. 6, the FB-layer needs more iterations to reach the same precision.

Let us consider now the differences between the PILE and the FB-layer methods. The two methods have different physical

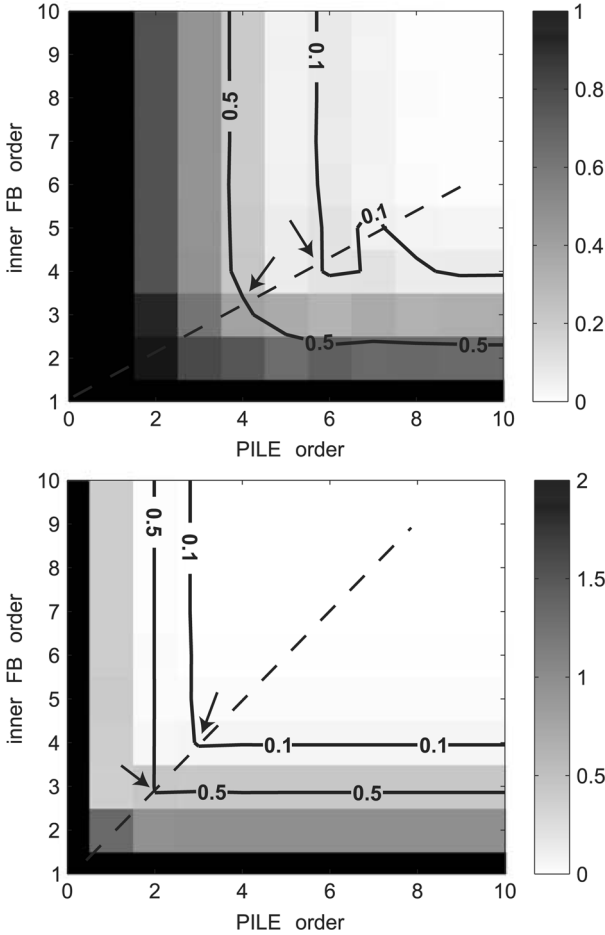


Fig. 7. Error on the bistatic scattering of the PILE-FBNSA versus the order P_{pile} of PILE method order and the order P_{fb} of FB used to speed up PILE. The parameters are: (top, case 1): $\sigma_h^A = \sigma_h^B = 0.4\lambda$, $\sigma_p^A = \sigma_p^B = 0.2$, $H = 1\lambda$, $\varepsilon_{r,1} = 2 + 0.01i$, $\theta_i = 0^\circ$, $L = 50\lambda$, $g = L/4$, TE polarization; (bottom, case 2): same as case 1, except: $\sigma_h^A = \sigma_h^B = 0.1\lambda$, $H = 3\lambda$. For both methods, $N_s^{A,B} = 50$ and $N_s^{\text{coupl}} = 50$. The optimal choices of P_{pile} and P_{fb} for a given error, are shown with an arrow.

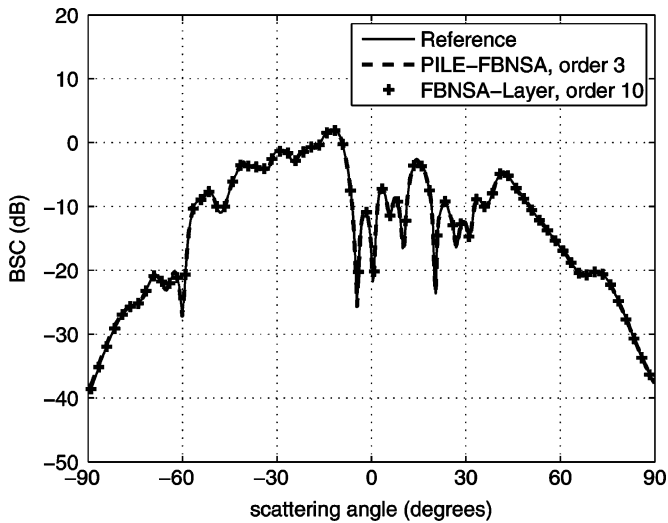


Fig. 8. Bistatic scattering coefficient from the PILE-FBNSA and the FBNSA-layer methods. The parameters are: $\sigma_h^A = \sigma_h^B = 0.5\lambda$, $\sigma_p^A = \sigma_p^B = 0.2$, $P_{\text{pile}} = 3$ and inner FB at order $P_{fb} = 5$; for FBNSA, $P_{\text{fblayer}} = 10$. For both methods, $N_s^{A,B} = 50$ and $N_s^{\text{coupl}} = 150$. $\theta_i = 0^\circ$, $g = L/6$ and $L = 50\lambda$, $\varepsilon_{r,1} = 2 + 0.01i$. Mean thickness $H = 5\lambda$.

interpretations, and thus the validity domains are *a priori* different.

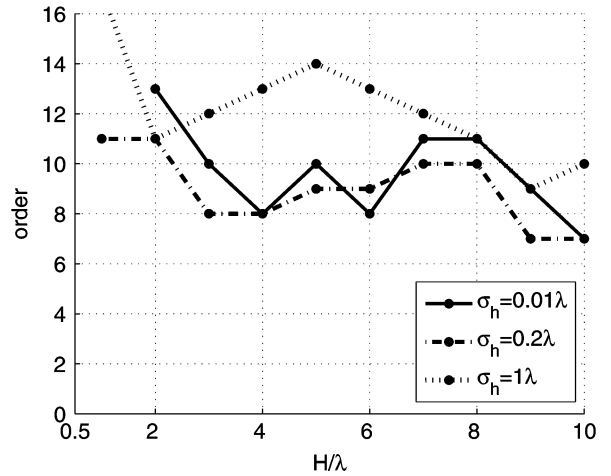


Fig. 9. Order of convergence of exact FB to reach an error of 0.1 dB on the BSC. $L = 50\lambda$. Rms heights $\sigma_h = \sigma_h^A = \sigma_h^B$, rms slopes $\sigma_p^A = \sigma_p^B = 0.2$, $\theta_i = 0^\circ$. TE case. $\varepsilon_{r,1} = 2 + 0.01i$.

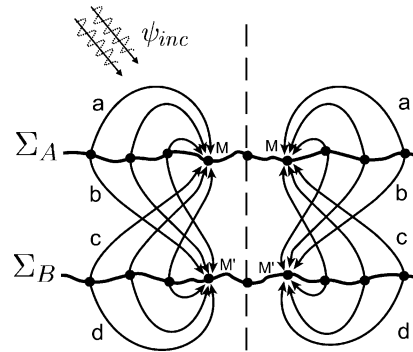


Fig. 10. Physical scheme of the FB method for a layer. Forward propagation (left), Backward propagation (right). M and M' are the current points; the impedance matrices corresponding to the steps are: step a), Z^A ; step b), $C^{A \rightarrow B}$; step c), $C^{B \rightarrow A}$; step d), Z^B .

The physical interpretation of the FB is shown in Fig. 10 for the dielectric layer case. This interpretation can be deduced from the block partitioning of the total impedance matrix of the layer (7). Let denote M and M' the current points on Σ_A and Σ_B , respectively. On the forward step, the field on M is deduced from the incident field on M and from the field on the points on its left, from both the upper and the lower interfaces. The difference with the PILE method is that the local interactions on each interface and the coupling between interfaces are derived at the same time. Hence, the FB for a layer seems able to take into account the multiple reflexions in the layer in few sweeps forward and backward across the surface.

However, system (12) on which FB is based was not derived rigorously, to our knowledge. Only a proof with a physical basis can be found in [44, Sec. 3], valid for a single interface and for grazing angles. Thus, the validity domain of FB method is still unclear; some criterion has to be found from which one would know if the FB will converge for a particular configuration. For this purpose, let us recall the original system of the FB (12)

$$Z^d X^f = s - Z^f (X^b + X^f) \quad (35)$$

$$Z^d X^b = -Z^b (X^b + X^f) \quad (36)$$

Initially, $\mathbf{X}^b = \mathbf{0}$. Hence, from (35)

$$\mathbf{X}^{f,(0)} = (\mathbf{Z}^d + \mathbf{Z}^f)^{-1} \mathbf{s} \quad (37)$$

and then from (36)

$$\mathbf{X}^{b,(0)} = -(\mathbf{Z}^d + \mathbf{Z}^b)^{-1} \mathbf{Z}^b (\mathbf{Z}^d + \mathbf{Z}^f)^{-1} \mathbf{s} \quad (38)$$

so

$$\begin{aligned} \mathbf{X}^{(0)} &= \mathbf{X}^{f,(0)} + \mathbf{X}^{b,(0)} \\ &= [\mathbf{I} - (\mathbf{Z}^d + \mathbf{Z}^b)^{-1} \mathbf{Z}^b] (\mathbf{Z}^d + \mathbf{Z}^f)^{-1} \mathbf{s}. \end{aligned} \quad (39)$$

By recurrence, from (35)–(36), for $p \geq 1$

$$\mathbf{X}^{f,(p)} = (\mathbf{Z}^d + \mathbf{Z}^f)^{-1} (\mathbf{s} - \mathbf{Z}^f) \mathbf{X}^{b,(p-1)} \quad (40)$$

$$\mathbf{X}^{b,(p)} = -(\mathbf{Z}^d + \mathbf{Z}^b)^{-1} \mathbf{Z}^b \mathbf{X}^{f,(p-1)}. \quad (41)$$

Introducing the expressions of $\mathbf{X}^{f,(0)}$ and $\mathbf{X}^{b,(0)}$ in (40) and (41), we deduce $\mathbf{X}^{f,(p)}$, $\mathbf{X}^{b,(p)}$ and $\mathbf{X}^{(p)}$, for $p > 1$. $\mathbf{X}^{(p)}$ can be cast into an expression similar than (8). At order P_{fblayer} for example

$$\mathbf{X}^{(P_{\text{fblayer}})} = [\mathbf{I} - (\mathbf{Z}^d + \mathbf{Z}^b)^{-1} \mathbf{Z}^b] \mathbf{s} \sum_{p=0}^{P_{\text{fblayer}}} \mathbf{Y}^{(p)} \quad (42)$$

where

$$\begin{aligned} \mathbf{Y}^{(0)} &= (\mathbf{Z}^d + \mathbf{Z}^f)^{-1} \mathbf{s} \quad \text{for } p = 0 \\ \mathbf{Y}^{(p)} &= \mathbf{M}_{\text{fblayer}} \cdot \mathbf{Y}^{(p-1)} \quad \text{for } p > 0, \end{aligned} \quad (43)$$

and

$$\mathbf{M}_{\text{fblayer}} = (\mathbf{Z}^d + \mathbf{Z}^f)^{-1} \mathbf{Z}^f (\mathbf{Z}^d + \mathbf{Z}^b)^{-1} \mathbf{Z}^b. \quad (44)$$

$\mathbf{M}_{\text{fblayer}}$ is the characteristic matrix of the layer for the FB algorithm. As for the characteristic matrix \mathbf{M}_c of PILE method (10), the product by $\mathbf{M}_{\text{fblayer}}$ requires 2 inversions and 2 multiplications.

It is interesting to calculate the spectral radius $\|\cdot\|$ of $\mathbf{M}_{\text{fblayer}}$. If this norm is bigger than 1, the sum in (42) is likely to diverge. Fig. 11 shows the values of $\|\mathbf{M}_{\text{fblayer}}\|$ and $\|\mathbf{M}_c\|$ versus the mean thickness H of the layer, for the following parameters: rms heights, $\sigma_h^A = \sigma_h^B = 0.01\lambda$, rms slopes $\sigma_p^A = \sigma_p^B = 0.2$, total length of both interfaces $L = 50\lambda$; TE case. The norm is independent of the incident angle.

From Fig. 11, the norm of both matrices increases when the thickness is small. However, the norm of PILE matrix is smaller than the one of FB, and this is always verified, whatever the parameters of the surfaces. This explains why PILE converges faster than FB.

To verify that the FB method diverges if $\|\mathbf{M}_{\text{fblayer}}\| > 1$, or equivalently, if $\mathbf{M}_{\text{fblayer}}$ has an eigenvalue bigger than 1 in modulus, we plotted $\|\mathbf{M}_{\text{fblayer}}\|$ and another criterion in Fig. 12.

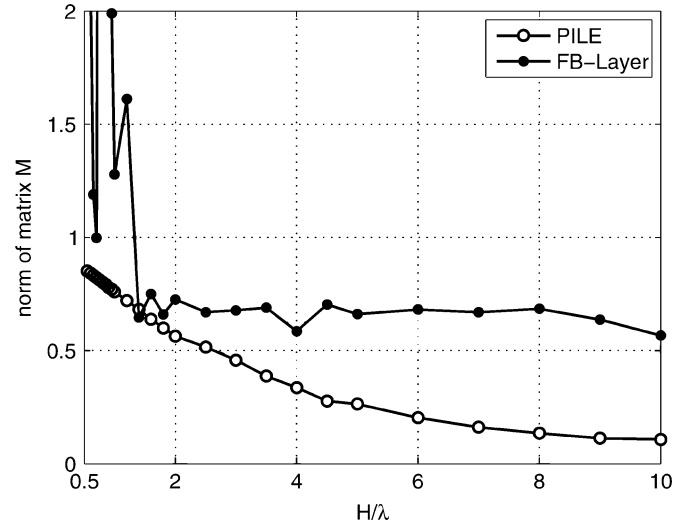


Fig. 11. Norm of the characteristic matrices $\mathbf{M}_{\text{fblayer}}$ and \mathbf{M}_c for the FB-layer and PILE methods, respectively. The parameters are: $\sigma_h^A = \sigma_h^B = 0.01\lambda$, $\sigma_p^A = \sigma_p^B = 0.2$. $L = 50\lambda$. TE case. $\varepsilon_{r,1} = 2 + 0.01i$.

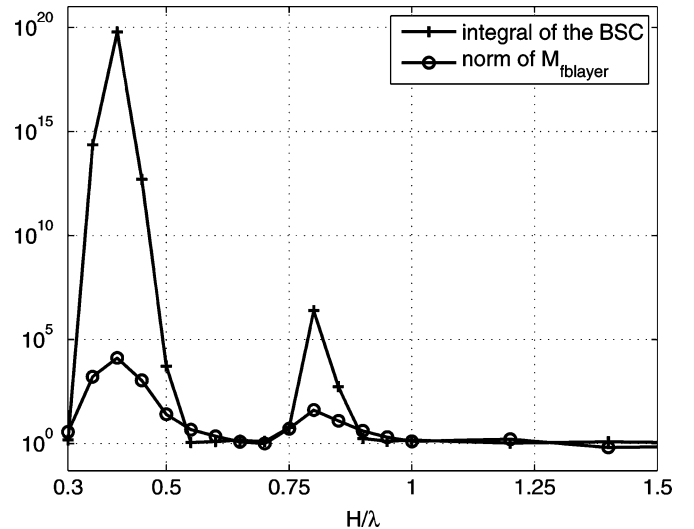


Fig. 12. Integral of the Bistatic Scattering Coefficient and norm of the characteristic matrix $\mathbf{M}_{\text{fblayer}}$ of the FB-layer method, order 3. The parameters are: $\sigma_h^A = \sigma_h^B = 0.01\lambda$, $\sigma_p^A = \sigma_p^B = 0.2$. $L = 50\lambda$. TE case. $\varepsilon_{r,1} = 2 + 0.01i$.

This criterion is based on the energy conservation, and more precisely on the integral of the bistatic scattering coefficient. This integral has to be equal or less than 1. The parameters considered are the same as in Fig. 11, and $\theta_i = 0^\circ$. The incident beam is a Thorsos beam, with $g = L/6$.

After 3 iterations of FB, the integral reaches high values, and this effect is even more marked when the number of iterations increases. That means that for the corresponding values of the mean thickness H , the FB does not converge. It is worth noticing that these peaks on the value of the criterion corresponds to the value peaks of the norm $\|\mathbf{M}_{\text{fblayer}}\|$. Hence, according to Fig. 12 and to other studies with different configurations, not shown here, the condition

$$\|\mathbf{M}_{\text{fblayer}}\| > 1 \quad (45)$$

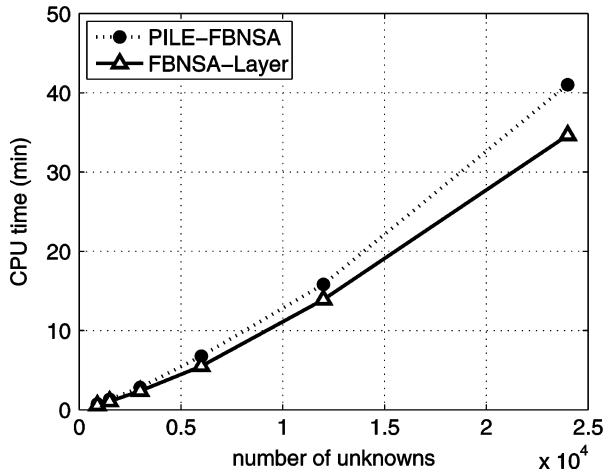


Fig. 13. CPU time of PILE-FBNSA and FBNSA for the given set of parameters: $P_{\text{pile}} = 4$ and inner FB at order $P_{fb} = 5$; for FBNSA, $P_{\text{fb}} = 10$. For both methods, $N_s^{A,B} = 50$ and $N_s^{\text{coupl}} = 50$.

is a condition of convergence of the FB method, where $\|\cdot\|$ is the spectral radius.

Thus, considering Fig. 11, the norm of $M_{\text{fb}}^{\text{layer}}$ is bigger than 1 when $H < 1.5\lambda$; this explains why the FB method diverges for small values of H in Fig. 9: the solid line, corresponding to $\sigma_h^{A,B} = 0.01\lambda$, and $\sigma_p^{A,B} = 0.2$ is not defined for $H < 2\lambda$. In fact, for $1.5\lambda < H < 2\lambda$ the FB converges in more than 20 iterations. In comparison, $M_c < 1$ for PILE, for $H > 0.5\lambda$, and accordingly, PILE method converges (solid line of Fig. 6), for all these values of H .

C. Computation Time

Simulations have been made for a typical configuration, where PILE method converges faster than the FB, that is for PILE-FBNSA, $P_{\text{pile}} = 4$ and inner FB at order $P_{fb} = 5$; for FBNSA-layer, $P_{\text{fb}} = 10$. For both methods, $N_s^{A,B} = 50$ and $N_s^{\text{coupl}} = 150$. The CPU time spent for each method is shown in Fig. 13. The number of unknowns is equal to $3N$ where N is the number of samples per interface, considering the layered PC case (Fig. 3). A 3 GHz personal computer with 2 GB of RAM is used in this work. We can verify from a linear regression that the CPU time of the PILE-FBNSA is approximately proportional to $\mathcal{O}(N)$. The slight discrepancy comes from the extra time needed to store the band matrices of strong interactions.

VI. CONCLUSION

We presented in this paper a new efficient method to predict the field scattered from a 1-D stack of two rough interfaces. The method is based on the rigorous PILE method [18], and it was accelerated using the fast method FBNSA of a single interface. Then the NSA was used to speed up the calculation of the coupling interactions between the two interfaces. The resulting method, the PILE-FBNSA, has a complexity of only $\mathcal{O}(N)$.

Then a numerical validation of the PILE-FBNSA was undertaken comparing it to a reference method, and to the recent FB for a layer [20]. The underlying physical interpretation of the

PILE method is different than for the FB method [20], and the validity domains are also different. A criterion on the convergence of FB was found.

The convergence of PILE-FBNSA has been established for layers with a thickness of 10λ and up; in some cases the PILE method converged whereas the FB method did not. Hence, the two methods PILE-FBNSA and FBNSA-layer are equivalent in time computation, but PILE-FBNSA is more robust when the layer is about one wavelength thick, and when guided waves exist. However, FBNSA has been derived for several layers, but no convergence study has been made for more than two interfaces.

REFERENCES

- [1] C. Amra, G. Albrand, and P. Roche, "Theory and application of antiscattering single layers: Antiscattering antireflection coatings," *Appl. Opt.*, vol. 16, pp. 2695–2702, 1986.
- [2] C. Amra, "Light scattering from multilayer optics. I. Tools of investigation," *J. Opt. Soc. Amer. A*, vol. 11, pp. 197–210, 1994.
- [3] C. Amra, "Light scattering from multilayer optics. II. Application to experiment," *J. Opt. Soc. Am. A*, vol. 11, pp. 211–226, 1994.
- [4] I. Ohlidal and K. Navratil, "Scattering of light from multilayer systems with rough boundaries," *Phys. Opt.*, vol. 34, pp. 251–334, 1995.
- [5] H. Kaplan, "Black coatings are critical in optical design," *Photon. Spectra*, vol. 31, pp. 48–50, 1997.
- [6] R. Garcia-Llamas, L. E. Regalado, and C. Amra, "Scattering of light from a two-layer system with a rough surface," *J. Opt. Soc. Am. A*, vol. 16, no. 11, pp. 2713–2719, 1999.
- [7] A. Soubret, "Diffusion Des Ondes Electromagnétiques Par Des Milieux et Des Interfaces Aléatoires: Étude Des Effets Cohérents Dans le Champ Diffusé," Ph.D. dissertation, Université de la Méditerranée, 2001, Aix-Marseille II, Centre de Physique théorique.
- [8] A. Madrazo and A. A. Maradudin, "Numerical solutions of the reduced Rayleigh equation for the scattering of electromagnetic waves from rough dielectric films on perfectly conducting substrates," *Opt. Commun.*, vol. 134, pp. 251–263, 1997.
- [9] V. Wismann, M. Gade, W. Alpers, and H. Hühnerfuss, "Radar signatures of marine mineral oil spills measured by an airborne multiradar," *IJRM*, vol. 19, pp. 3607–3623, 1998.
- [10] H. A. Espedal and O. M. Johannessen, "Detection of oil spills near offshore installations using synthetic aperture radar (SAR)," *IJRM*, vol. 21, pp. 2141–2144, 2000.
- [11] Z. Otremba and J. Piskozub, "Modelling of the optical contrast of an oil film on a sea surface," *OE*, vol. 9, no. 12, pp. 411–416, 2001.
- [12] D. Goodman and Conyers, *Ground Penetrating Radar, An Introduction for Archaeologists*. Walnut Creek, CA: Altramira Press.
- [13] A. Tabatabaenejad and M. Moghaddam, "Bistatic scattering from three-dimensional layered rough surfaces," *IEEE Trans. Geos. Remote Sensing*, vol. 44, no. 8, pp. 2102–2114, 2006.
- [14] A. Soubret, G. Berginc, and C. Bourrelly, "Backscattering enhancement of an electromagnetic wave scattered by two-dimensional rough layers," *J. Opt. Soc. Am. A*, vol. 18, pp. 2778–2788, 2001.
- [15] Y. Altuncu, A. Yapar, and I. Akduman, "On the scattering of electromagnetic waves by bodies buried in a half-space with locally rough interface," *IEEE Trans. Geos. Remote Sens.*, vol. 44, no. 6, pp. 1435–1443, 2006.
- [16] Y. Altuncu, A. Yapar, and I. Akduman, "Buried object approach for solving scattering problems related to rough surfaces," *Canadian J. Phys.*, vol. 85, no. 1, pp. 39–55.
- [17] N. Pinel, N. Déchamps, C. Bourlier, and J. Saillard, "Bistatic scattering from one-dimensional random rough homogeneous layers in the high-frequency limit with shadowing effect," *Waves in Random Complex Media*, to be published.
- [18] N. Déchamps, N. De Beaucaudrey, C. Bourlier, and S. Toutain, "Fast numerical method for electromagnetic scattering by rough layered interfaces: Propagation-inside-layer expansion method," *J. Opt. Soc. Am. A*, vol. 23, no. 2, pp. 359–369, 2006.
- [19] C.-H. Kuo and M. Moghaddam, "Scattering from multilayer rough surfaces based on the extended boundary condition method and truncated singular value decomposition," *IEEE Trans. Antennas Propag.*, vol. 54, no. 10, pp. 2917–2929, 2006.

- [20] C. D. Moss, T. M. Grzegorzczak, H. C. Han, and J. A. Kong, "Forward-backward method with spectral acceleration for scattering from layered rough surfaces," *IEEE Trans. Antennas Propag.*, vol. 54, no. 10, pp. 2917–2929, 2006.
- [21] M. El-Shenawee, "Polarimetric scattering from two-layered two-dimensional random rough surfaces with and without buried objects," *IEEE Trans. Geos. Rem. Sens.*, vol. 42, no. 1, pp. 67–76, 2004.
- [22] F. Harrington, *Field Computation by Moment Methods*. Piscataway, NJ: IEEE Press, 1993.
- [23] L. Tsang, J. A. Kong, K.-H. Ding, and C. O. Ao, *Scattering of electromagnetic waves: Numerical simulations*. New York: Wiley Interscience, 2001.
- [24] M. Saillard and A. Sentenac, "Rigorous solution for electromagnetic scattering from rough surfaces," *Waves in Random Media*, vol. 11, pp. R103–R137, 2001.
- [25] K. F. Warnick and W. C. Chew, "Numerical simulation methods for rough surface scattering: Topical review," *Waves in Random Media*, vol. 11, pp. R1–R30, 2001.
- [26] C. S. West and K. A. O'Donnell, "Observations of backscattering enhancement from polaritons on a rough metal surface," *J. Opt. Soc. Am. A*, vol. 12, no. 2, pp. 390–397, 1995.
- [27] E. I. Thorsos, "The validity of the Kirchhoff approximation for rough surface scattering using a Gaussian roughness spectrum," *J. Acoust. Soc. Am.*, vol. 83, no. 1, pp. 78–92, 1988.
- [28] J. Q. Lu, A. A. Maradudin, and T. Michel, "Enhanced backscattering from a rough dielectric film on a reflecting substrate," *J. Opt. Soc. Am. B*, vol. 8, no. 2, pp. 311–318, 1991.
- [29] V. Freilikher, E. Kanziiper, and A. A. Maradudin, "Coherent scattering enhancement in systems bounded by rough surfaces," *Phys. Reports*, vol. 288, pp. 127–204, 1997.
- [30] M. Saillard and G. Toso, "Electromagnetic scattering from bounded of infinite subsurface bodies," *Radio Sci.*, vol. 32, no. 4, pp. 1347–1359, 1997.
- [31] W. H. Press, S. A. Teukolsky, W. T. Vetterling, and B. P. Flannery, *Numerical Recipes*, 2nd ed. Cambridge: Cambridge Univ. Press, 1992.
- [32] L. Tsang, C. H. Chan, K. Pak, and H. Sangani, "Monte-Carlo simulations of large-scale problems of random rough surface scattering and applications to grazing incidence with the BMIA/Canonical grid method," *IEEE Trans. Antennas Propag.*, vol. 43, pp. 851–859, 1995.
- [33] J. T. Johnson, "On the canonical grid method for two-dimensional scattering problems," *IEEE Trans. Antennas Propag.*, vol. 46, no. 3, pp. 297–302, 1998.
- [34] C. H. Chan, L. Tsang, and Q. Li, "Monte-Carlo simulations of large-scale one-dimensional random rough-surface scattering at near-grazing incidence: Penetrable case," *IEEE Trans. Antennas Propag.*, vol. 46, no. 1, pp. 142–149, 1998.
- [35] Q. Li, C. H. Chan, and L. Tsang, "Monte-Carlo simulations of wave scattering from lossy dielectric random rough surfaces using the physics-based two-grid method and the canonical-grid method," *IEEE Trans. Antennas Propag.*, vol. 47, no. 4, pp. 752–763, 1999.
- [36] D. J. Donohue, H.-C. Ku, and D. R. Thompson, "Application of iterative moment-method solutions to ocean surfaces radar scattering," *IEEE Trans. Antennas Propag.*, vol. 46, no. 1, pp. 121–132, 1998.
- [37] V. Rokhlin, "Rapid solution of integral equations of scattering theory in two dimensions," *J. Comput. Phys.*, vol. 36, pp. 414–439, 1990.
- [38] D. Holliday, L. L. DeRaad Jr., and G. J. St-Cyr, "Forward-backward method for scattering from imperfect conductors," *IEEE Trans. Antennas Propag.*, vol. 46, no. 1, pp. 101–107, 1998.
- [39] H.-T. Chou and J. T. Johnson, "A novel acceleration algorithm for the computation of scattering from rough surfaces with the forward-backward method," *Radio Sci.*, vol. 33, pp. 1277–1287, 1998.
- [40] H.-T. Chou and J. T. Johnson, "Formulation of forward-backward method using novel spectral acceleration for the modeling of scattering from impedance rough surfaces," *IEEE Trans. Geos. Rem. Sens.*, vol. 38, no. 1, pp. 605–607, 2000.
- [41] D. Torrungrueng and J. T. Johnson, "Some issues related to the novel spectral acceleration method for the fast computation of radiation/scattering from one-dimensional extremely large scale quasi-planar structures," *Radio Sci.*, vol. 37, no. 2, 2002.
- [42] A. Iodice, "Forward-backward method for scattering from dielectric rough surfaces," *IEEE Trans. Antennas Propag.*, vol. 50, no. 7, pp. 901–911, 2002.
- [43] N. Déchamps and C. Bourlier, "Electromagnetic scattering from a rough layer: Propagation-inside-layer expansion method combined to an updated BMIA/CAG approach," *IEEE Trans. Antennas Propag.*, vol. 55, pp. 2790–2802, Oct. 2007.
- [44] D. Holliday, L. L. DeRaad, and G. J. St-Cyr, "Volterra approximation for low grazing angle shadowing on smooth ocean-like surfaces," *IEEE Trans. Antennas Propag.*, vol. 43, no. 11, pp. 1199–1205, 1995.



Nicolas Déchamps was born in Provins, France, in 1977. He received the Engineering Degree from Ecole Centrale de Nantes, Nantes, France, the M.Sc. degree in automation and applied computer science from the Communications and Cybernetic Research Institute of Nantes (IRCCyN), and the Ph.D. degree in physics from the Institut de Recherche en Electrotechnique et Electronique de Nantes Atlantique, (IREENA), in 2001 and 2004, respectively.

After a postdoctoral position at the Pulp and Paper Center at the University of Toronto, Canada, where he worked on optical properties of paper, he joined the radar team of IREENA Laboratory as a Research Associate in 2006. His research interest includes fast methods for numerical simulations of scattering from multilayers separated by rough interfaces and analytical modelling of paper gloss.



Christophe Bourlier (M'99) was born in La Flèche, France, on July 6, 1971. He received the M.S. degree in electronics from the University of Rennes, Rennes, France, in 1995 and the Ph.D. degree from the Système Electronique et Informatique (SEI), Nantes, France, in 1999.

While at the University of Rennes, he was with the Laboratory of Radiocommunication where he worked on antennas coupling in the VHF-HF band. Currently, he is with the IREENA Laboratory (Institut de Recherche en Electrotechnique et Electronique de Nantes Atlantique, France) with the radar team at Polytech Nantes (University of Nantes, France). He works as an Assistant Researcher with the National Center for Scientific Research on electromagnetic wave scattering from rough surfaces and objects for remote sensing applications. He is the author of more than 80 journal articles and conference papers.